The Use of Ni/Sb – SnO_2-based Membrane Electrode Assembly for Electrochemical Generation of Ozone and the Decolourisation of Reactive Blue 50 Dye Solutions

Khalid Zakaria [a], Paul Andrew Christensen*[b]

[a] *School of Civil Engineering and Geosciences, Bedson Building, Newcastle University, Newcastle upon Tyne, NE1 7RU*

[b] *School of Chemical Engineering and Advanced Materials, Bedson Building, Newcastle University, Newcastle upon Tyne, NE1 7RU- Email: Paul.Christensen@newcastle.ac.uk*

Tel: +44 (0) 191 222 5472

Abstract

Electrochemical ozone generation with ozone current efficiencies up to 33% and power consumption as low as 25 kWh kg^{-1} O_3 at room temperature using Ni/Sb-SnO_2 anodes in a membrane electrode assembly (MEA) based cell with platinised titanium cathodes separated by Nafion membrane is reported. The complete decolourisation of 200 cm^3 of 1000 mg dm^{-3} Reactive Blue 50 (RB50) dye within 8 minutes at 2.7 V with 100% current efficiency for the first 5 minutes and specific power consumption as low as ca. 8 kWh kg_{COD}^{-1} using the MEA – based cell is also described. The byproducts of the dye oxidation were investigated and the formation of various organic acids confirmed.

Keywords:

Ozone, MEA, Decolourisation, Electrolysis, Ozonation.

1 Introduction

To date, electrochemical technologies for wastewater treatment have developed such that

23 they are more efficient and more compact than other technologies, but cost is still an issue [1].
24 Highly efficient chemical oxidants such as ozone, hydroxyl radicals or hydrogen peroxide
25 can be generated electrochemically [2]. Electrochemical oxidation is a popular
26 electrochemical procedure for removing organic pollutants, such as dyes [3], from industrial
27 wastewaters [4]. The electrochemical oxidation of pollutants can be either direct or indirect
28 [3-7]. During indirect oxidation at the electrode/electrolyte interface, organic molecules are
29 attacked by electrogenerated oxidants, while in direct electro-oxidation, organics are attacked
30 at the anode surface by chemisorbed, active oxygen species [8, 9].

31 The electrochemical generation of ozone has many advantages over conventional ozone
32 generators, such as Cold Corona Discharge or Dielectric Barrier Discharge units [10],
33 including: low voltage operation, the possibility of generating high concentrations of ozone in
34 the gas and liquid phases with very high ozone current efficiency, no need for gas feeds of
35 any description and robust and simple system design [11].

36 Ni/Sb-SnO_2 (NATO) ozone anodes have been reported to show high ozone current
37 efficiencies for the production of ozone at room temperature in acidic electrolytes [11-17] or
38 de-ionised water [16, 18], with ozone current efficiencies up to 50% [11, 16].

39 There are a number of types of electrochemical cell employed in the electrochemical
40 generation of ozone [16]. Such cells fall broadly into two categories: single compartment [12,
41 13] and two compartments [11, 19]; the compartments of the latter are separated by a
42 membrane that is either porous or an ionic conductor such as Nafion (as an example of a
43 Polymer Electrolyte Membrane or PEM) [18].

44 In contrast to, for example PbO_2 [20], NATO anode – based MEA cells have not been
45 researched extensively with respect to ozone generation. The only such work reported in the
46 literature was carried out by the Chan group in Hong Kong University [18, 19] using 24 cm^2

47 [19] or 104 cm^2 [18] NATO anodes on Ti mesh (ca. 50% open area). Thus, the chan group
48 [19] reported a ozone current efficiency of 15% at 2 V and ca.13 mA cm^{-2} using a single cell
49 and static deionised (DI) water as anolyte. With 104 cm^{-2} NATO anodes and flowing DI
50 water as anolyte, efficiencies up to 17% at ca. 3 V and 19.2 mA cm^{-2} with a single cell, and
51 22% at ca. 3 V and ca. 30 mA cm^{-2} for a 4 – cell stack were reported [18].

52 Ozone has been extensively investigated with respect to the oxidative treatment of water and
53 wastewater [21], reacting with a large number of organic compounds either by direct
54 oxidation as molecular ozone (in acidic solutions) or by indirect oxidation through the
55 formation of secondary oxidants such as hydroxyl radicals (in alkaline solutions) [22].

56 Wastewater containing organic dyes is becoming an increasing problem worldwide due to the
57 extensive use of these compounds, with production estimated at over 7×10^5 tons/annum [4,
58 23, 24].

59 The main characteristic of dyes is the chromophore group which includes: azo (– N = N –),
60 antraquinone, indigoide, etc derivatives [25]. A polyaromatic structure, high molecular
61 weight and atoms of nitrogen, sulphur and metals are characteristics of most dye molecules
62 [22]. Dyes can be reactive, direct, etc according to the method by which they are fixed on
63 fibres [26]. For example, reactive dyes are designed to improve colour fastness as they have
64 functional groups in their structure which form covalent bonds with fibres [27]. Over 20-25 %
65 of reactive dyes are lost from the dyeing process and leave with the wastewater [1]. As an
66 example of a reactive dye, Reactive Blue 50 dye was studied in the work presented in this
67 paper.

68 In general, conventional wastewater treatment plants are not capable of remediating dye-
69 containing wastewaters due to the high photochemical and thermal stability of such dyes, and
70 their resistance to microbial attack [4, 22-24]. As a result, there has been increasing interest

in other methods to decolourise and degrade dye wastewaters such as: physico-chemical techniques [4, 7, 28]; Advanced Oxidation Processes (AOPs) [4, 7, 25, 29]; membranes [4] and electrochemical technologies [4-7, 29, 30].

It has been found that the nature of the anode material influences strongly both the selectivity and efficiency of the electrochemical oxidation process. Comninellis [8] divided the behaviour of the anodes in electrochemical oxidation into two types: active and inactive. Typical examples of the former are: Pt, IrO_2 and RuO_2 [4, 30, 31] and of the latter: PbO_2, SnO_2 and BDD [4, 30, 31]. Inactive electrodes do not participate in the oxidation of organics and do not provide any catalytically active site for their adsorption from aqueous media [4, 30, 31], acting only as an inert source and sink for electrons; in contrast, active anodes participate directly in organic oxidation, with the oxidation byproducts adsorbing on the anode surface [4, 30, 31].

For some industrial wastewaters, electrochemical technologies may be the indispensable step in the treatment of refractory pollutants [6]. The main advantage of electrochemical methods is that added chemicals are not required and sludge is not produced [23].

The aim of the work reported in this paper was to investigate the electrochemical generation of ozone at NATO anodes in a Membrane Electrode Assembly (MEA) – based cell, and to explore the decolourisation of Reactive Blue 50 (RB50) dye solutions in the MEA cell.

2 Experimental

2.1 Chemicals

$HClO_4$ (Puriss, Fluka) and Reactive Blue 50 (RB50) dye (Langholm Dying Company, Scotland) were used as received without further purification. Millipore Milli-Q water (18 MΩ

93 cm) was used to prepare all solutions. Table 1 shows the molecular formula and structure of
94 the RB50.

95 2.2 Electrode Preparation

96 The catalysts were prepared according to the methodology reported previously by
97 Christensen et al. [14] by dipcoating onto 7.0 cm × 5.0 cm Ti mesh (ca. 50% open area)
98 substrates (Dexmet, USA) from ethanolic solutions of the Sn, Sb and Ni metal salts. The
99 concentrations of Sn: Sb: Ni in the coating solutions were 93.0 at.%:6.0 at.%: 1.0 at.%. The
100 coating cycle was repeated 20 times [11, 32]).

101 A 7.0 cm × 5.0 cm platinised Ti mesh (Pt/Ti) (50% open area) was employed as the counter
102 electrode (NRK Electrochem).

103 The 7.0 cm × 5.0 cm anodes and cathodes were spot welded into a titanium frame, giving an
104 active area of 6 cm × 4 cm, see figs 1(a) and (b).

105 2.3 Membrane Electrode Assembly

106 The Membrane Electrode Assembly was fabricated by hot-pressing (Elcometer, heated press /
107 250 ^{O}C / 30000 N) the framed NATO mesh anode and framed Pt/Ti mesh cathode either side
108 of 5 cm × 7 cm Nafion 117 membrane (DuPont Corp., USA) at 150 ºC and 800 N for 3
109 minutes, after which the MEA was turned through 180º and the process repeated.

110 The MEA was mounted between the cathodic and anodic compartments (each ca. 10 cm^3
111 volume) of the polycarbonate cell, with sealing maintained using silicon “O” rings. A
112 schematic representation of the polycarbonate cell and the MEA are shown in fig. 1(a) and
113 anode and cathode with the Ti frames are in fig. 1(b).

2.4 The Ozone Generation System

The flow (single pass) system is shown elsewhere (see Christensen et al [14]), which employed the polycarbonate cell housing the MEA.

An aqueous solution of 1 M $HClO_4$, or water from the Millipore Milli – Q system were employed as the anolyte and/or catholyte, which were kept separate by the MEA. The catholyte was stationary and supplied from a glass reservoir via polyethylene (PE) tubing (Portex 800/012/425/800 7.0 mm x 10.5 mm). The anolyte was pumped in the flow system through the anodic compartment of the polycarbonate cell using a Masterflex Digital Standard Cartridge Pump (Cole-Palmer) via PE tubing. The cell voltage or current density were controlled with a TTi TSX 1820P programmable DC power supply unit (PSU).

A Cole- Palmer WU series flowmeter was used to control the flowrate of nitrogen gas from a cryogenic boil-off which was employed to dilute the ozone gas generated by the MEA. The ozone then exhausted into a fume hood.

2.5 Ozone Measurement

Both gaseous and dissolved ozone were monitored using (b = 1 cm) pathlength UV-Vis cells (Astranet), and Astranet UV-Vis fibre optic spectrometer systems (Cambridge, UK). The value employed for the extinction coefficient ϵ of gas and solution phase ozone at ca. 255 nm and 258 nm was 3000 mol^{-1} dm^3 cm^{-1} [33].

Ozone concentration (mg dm^{-3}) = A.48.1000/ϵ.b = 16.A (1)

The ozone current efficiency can be calculated from [14]:

$$\eta(\%) = 0.32Af/I \quad (2)$$

Where A is the ozone absorbance in the solution or gas phases, *f* is the anolyte flow rate or

136 the nitrogen + ozone flow rate (for gas phase) in cm^3 min^{-1} and I is the current (A). The
137 derivation of equation (2) is presented elsewhere [14]. All experiments were conducted at
138 room temperature, 20–25 ^{O}C.

139 The ozone production rate (OPR) was calculated according to:

140 $$OPR\ (mg\ h^{-1}\ cm^{-2}) = I.\eta.t.48.1000.3600/6F.a = 299.I.\eta/a \qquad (3)$$

141 Where: η is the ozone current efficiency (as a decimal), t is the time (s), 48 is the molecular
142 weight of ozone (g mol^{-1}), 6 is the number of electrons involved, F is Faraday's constant
143 (96480 C mol^{-1}) and a is the electrode geometric area (24 cm^2).

144 The power consumption was calculated from:

145 $$P\ (kWh\ kg_{O3}^{-1}) = 3.35\ V/\eta \qquad (4)$$

146 Where V is the cell voltage (V).

147 **2.6 Decolourisation**

148 The system used for decolourisation is shown in fig. 2 and was operated in recycle mode;
149 thus, 200 cm^3 of the stock RB50 solution, as anolyte, was recycled through the anodic
150 compartment of the MEA – based cell using a peristaltic pump at recycle flow rate of 200
151 cm^3 min^{-1}. The solution then entered a gas separator to separate ozone bubbles from the
152 anolyte, the gas phase ozone in the separator was diluted and carried by N_2 gas through a 1
153 cm path length UV – Vis flow cell (Astranet). The catholyte was 1 M $HClO_4$, static and
154 supplied from a reservoir, and was kept separated from the dye solution by the MEA. The
155 various system components were connected by polyethylene (PE) tubes. Nitrogen gas from a
156 cryogenic boil-off was supplied at a carefully-controlled rate (typically 120 cm^3 min^{-1}) using
157 a Cole-Palmer WU series flow meter system. 200 cm^3 of 100 or 1000 mg dm^{-3} RB50 solution

158 was recycled at constant cell voltage of 2.7 V. Samples were withdrawn using a sampling
159 port (see fig. 2) at regular intervals during 60 minutes runs and the absorbance measured
160 using 1 cm path length quartz cuvette in a UV mini 1240 Shimadzu spectrophotometer.

161 When decolourising the 1000 mg dm^{-3} of dye solution, the absorbance of the solution was too
162 high to obtain meaningful data; hence 1 cm^3 samples of the dye solution were diluted by a
163 factor of 10 with Millipore water prior to obtaining UV – Vis spectra.

164 The Closed Reflux Titrimetric Method was used to measure chemical oxygen demand (COD,
165 procedure 5220 C, American Public Health Association [34]) and a Shimadzu TOC analyzer
166 5050 A ASI- 5000 was used for estimating the total organic carbon (TOC).

167 Intermediates were investigated using Ion Chromatography (IC) via a Dionex ICS-1000 with
168 an AS40 auto sampler. The column was an IonPac AS14A, 4x250mm analytical column. The
169 flow rate was 1ml/min, eluent was a 8.0mM Na_2CO_3/1.0mM $NaHCO_3$ solution. Injection
170 loop was 25ul.

171 ## 2.7 Calculations

172 ### *2.7.1 Removal Efficiency*

173 The UV – Vis spectrum of RB50 solution shows bands in the visible region (associated with
174 colour) and in the UV region (associated with aromatic rings); in particular, bands near 254
175 nm are associated with the benzene ring [23, 35, 36], and bands at 625 nm and 586 nm have
176 been attributed to the anthraquinone moiety of the dye, see table 1.

177 The removal efficiency for colour and benzene rings were determined as follows:

178

179 $$R(\%) = 100\ (A_0 - A_t)/A_0 \qquad (5)$$

180

Where: A_0 is the initial absorbance at 625 nm or 586 nm (colour), or 254 nm (benzene ring); A_t is the absorbance at 625 nm, 586 nm or 254 nm at time t for colour and aromatic rings, respectively. 100% benzene ring removal was defined as when the peak at 254 nm disappeared.

2.7.2 Current efficiency

The dye removal current efficiency can be calculated as follows [7]:

$$CE\ \% = F.V_e.(COD_0 - COD_t)/8.I.t \qquad (6)$$

Where: V_e is the electrolyte volume (dm^3), COD_0 and COD_t are the chemical oxygen demands at times t=0 and t, respectively.

2.7.3 Specific energy consumption

The specific energy consumption during the degradation of the dye can be estimated as follows [7]:

$$E_{sp} = F.V_c/3600.8.CE \qquad (7)$$

Where: V_c is the cell voltage.

3 Results and Discussion

3.1 Ozone Generation

Figure 3(a) shows the ozone concentration (in mg dm^{-3}) in the solution and gas phases, and the total concentration as a function of the cell voltage during ozone generation using the MEA in single pass (flow) experiments. The data points in fig. 3(a) represent steady state measurements after ≥ 15 minutes at that particular cell voltage. It may be seen from the figure that O_3 concentration in both phase increased with increasing cell voltage up to 2.8 V after which it reached a plateau. The ozone in solution phase was higher than that in the gas phase when the cell voltages was <2.8 V which most likely reflecting a delay caused by the

arrangement of the system. However, the ozone concentration in both phases was almost equal at cell voltages >2.7 V. The total concentration reached ca. 20 mg dm^{-3} at cell voltages >2.7 V. This concentration was comparable with that observed by Wang et al. [19],who reported 19 mg dm^{-3} in solution phase only with the anolyte pumped through the cell, using an MEA with an air breathing cathode and NATO anode (4 cm × 6 cm Ti mesh 50% open area) at 2 V. In this study, the authors reported that the ozone concentration in both phases increased with cell voltage up to 2 V after which it decreased at higher voltages. In another paper, Wang et al. [12] reported 34 mg dm^{-3} at 2.2 V vs. AgCl/Ag with static anolyte. They interpreted their data by stating that either more oxygen rather than ozone was produced or the ozone decomposed to oxygen at higher cell voltages.

Figure 3(b) shows the current density and ozone current efficiencies (solution, gas and total) vs. cell voltage for the experiments depicted in fig. 3(a). It may be seen from the figure that the current increased with increasing voltage up to 2.8 V, after which it increased more slowly. It is worth noting that other groups have not reported using such high current densities as the ones attained in the experiments depicted in fig. 3(b). Thus, the max current densities reported by Chan group are 58 mA cm^{-2} using MEA based cells [18] and 15 mA cm^{-2} using electrodes immersed directly in acid [12]. Ozone was produced at voltages > 2.3 V. The current efficiency for dissolved ozone increased to a value of ca. 25% at 2.5 V and then decreased with increasing voltage, whereas the gas phase ozone current efficiency increased slowly to ca. 10 % at 2.6 V, then remained steady with increasing voltage. The total ozone current efficiency simply reflects the sum of these two contributions. As may be seen from the figure, irrespective of the cell voltage, more ozone was entrained in the solution phase than the gas; however, higher cell voltage result in an increasing fraction of ozone in the gas phase at the expense of that dissolved in solution, as well as a general decline in total efficiency.

Given that the distribution of ozone between solution and gas depends upon the system, further discussion will focus only on the total ozone production. The maximum current efficiency was about 33% compared to 21% reported by K. Y. Chan group [18] using a NATO anode in the MEA cell and an air breathing cathode; to our knowledge, 33% is the highest reported to date using an MEA with NATO anodes. The variation in ozone current efficiency with cell voltage suggests that the ozone active sites on the anode surface were switched on at voltages > 2.3 V, and the ratio of ozone/oxygen active sites increased with increasing voltage between 2.3 – 2.5 V. However, at voltages > 2.5 V, the ratio of ozone/oxygen sites decreased with increasing voltage, or the amount of ozone produced was less due to: (i) local heating effects that increase with increasing current density leading to a decrease in ozone efficiency [19, 37, 38], (ii) the switching over of ozone active sites to oxygen [12, 19, 39], (iii) the decomposition of ozone as a result of its reaction with OH radicals:

$$OH^{\cdot} + O_3 \rightarrow O_2 + HO_2^{\bullet} \qquad (8)$$

with such radicals being produced at significant rates at higher current densities [19, 38, 40] and/or (iv) ozone decomposition:

$$O_3 + O_3 \rightarrow 3O_2 \qquad (9)$$

Equation (9) represents the sum of the equations given by Gardoni et al. [41] for ozone decomposition.

To the best of our knowledge, an MEA consisting of a NATO anode/Nafion117/Pt/Ti cathode has not been investigated for ozone generation previously. Therefore, it does not seem unreasonable to use the literature on MEA – based cells with anodes other than NATO as a

starting point for discussion.

The increase in current with voltage seen in fig. 3(b) was expected and has been reported by Wang et al. [19]. In a second paper, the same group [18] employed the MEA in a flow-through cell and applied constant current. They observed that the cell voltage increased with current density.

Ozone current efficiency passing through a maximum (see fig. 3(b)) with increasing current using MEA – based ozone cells has been reported many times for a range of different types of anode and cathode; see for example: Arihara et al. [42], Onda at al. [43] and Kraft et al. [38]. Kraft et al. [38] studied ozone generation from water (1 μS cm^{-1}) using boron doped diamond (BDD) anode and cathode, separated by Nafion N324 at 0.1 – 5 A in a flow – through reactor. The authors found that the current efficiency passed through a maximum at 1 – 1.5 A after which it decreased with increasing current. They interpreted the decrease in ozone current efficiency in terms of either: (i) the production of hydrogen peroxide accelerating ozone decomposition and/or (ii) local heating leading to lower ozone production or faster ozone decay.

Figure 3(c) shows the power consumption and ozone production rate for the experiments in fig 3(a). It may be seen from the figure that the power consumption decreased with increasing voltage to a value of ca. 25 kWh kg^{-1} O_3 at 2.5 V after which it increased almost linearly. This is in general agreement with the work of Stucki et al. [44] and Onda et al. [43] who used an MEA consisted of PbO_2 anode/Nafion 117/Pt cathode to generate ozone at constant current from water. The authors found that the power consumption decreased to a minimum (ca. 65 kWh kg^{-1} O_3 at about 1 A cm^{-2} [44] or ca. 130 kWh kg^{-1} O_3 at 1 A cm^{-2} [43]), after which it increased. In contrast, Arihara et al. [42] used an MEA consisting of a porous BDD plate anode and Pt mesh cathode from pure water at constant current of 1 – 10 A, and found

276 that the power consumption increased with increasing current. Da Silva et al. [20] using MEA
277 found that power consumption decreased with increasing current. Arihara et al. and Da Silva
278 et al. did not comment further on their data.

279 It may be seen from fig. 3(c) that the ozone production rate increased with increasing voltage
280 up to 2.8 V then remained almost constant. This behaviour is in general agreement with the
281 work of Kraft et al. [38] who reported that the ozone production rate increased with
282 increasing current. Arihara et al. [40] and Da Silva et al. [20] also found that the ozone
283 production rate increased with increasing current.

284 ### 3.2 Decolourisation of RB50 Solutions

285 In the first decolourisation experiment, 200 cm^3 of 100 mg dm^{-3} RB50 solution was
286 decolourised in the system depicted in fig. 2 at constant cell voltage of 2.7 V. Complete
287 decolourisation took place within 3 minutes, (data not shown). Hence the decolourisation of a
288 1000 mg dm^{-3} RB50 solution was investigated. Figure 4(a) shows the UV – Vis spectra of the
289 latter solution during electrolysis in the MEA – based electrochemical cell in recycle mode. It
290 may be seen from the figure that the spectrum of RB50 consists of three well – defined peaks,
291 at 254 nm, 586 nm and 625 nm. All three bands decreased with time. The loss of the UV
292 band near 254 nm suggest that the dye is being oxidised into fragments [45], while the
293 decrease in the intensities of the 625 nm and 586 nm bands may be attributed to the
294 destruction of the anthraquinone moiety [3].

295 Figure 4(b) shows plots of removal efficiencies of 254 nm, 586 nm and 625 nm bands as a
296 function of time during the experiment in fig. 4(a). As can be seen from the figure, the
297 decrease in intensity of the 586 nm and 625 nm features track each other as would be
298 expected, as they are due to the same anthraquinone chromophore. Therefore, the removal of
299 the 625 nm bands were taken as representative of colour removal. In addition, the decrease in

300 the intensity at and 254 nm was considered as representative of benzene ring removal. As can
301 be seen from fig. 4(b), the complete removal of both colour and the benzene ring was
302 achieved within 8 min. It is generally accepted that colour removal starts by the cleavage of
303 the chromophore [22].

304 The first step in electrochemical generation of ozone is generally believed to be the formation
305 of OH radicals [4, 8, 16, 17]:

306 $$H_2O \rightarrow HO^{\cdot} + H^{+} + e^{-} \qquad (8)$$

307 which can either be released from the electrode surface and react with dye molecules in the
308 near – electrode region, or oxidise adsorbed dye molecules. In general, reaction of OH
309 radicals with organic molecules includes hydrogen abstraction from and/or addition to
310 unsaturated (- C = C -) carbon double bonds [46]. Hence it would be expected that OH
311 radicals will attack the anthraquinone and benzene ring moieties, cleaving both. The cleavage
312 of the anthraquinone and the benzene ring result in the initial formation of smaller molecules,
313 mainly aliphatic acids [23]. It should be noted that the initial pH of the RB50 solution was
314 4.72 and decreased to 2 at the end of decolourisation process, confirming the formation of
315 acidic byproducts (see below).

316 Figure 5(a) shows the COD and TOC removal as a function of time for the experiments in fig.
317 4(a). It may be seen from the figure that both the COD and the TOC decreased with time with
318 more COD being removed. The decrease in COD and TOC reflect the degradation of the dye
319 molecules. From fig. 5(a), it can be seen that ca. 35% of the dye is degraded (i.e. oxidised to
320 smaller fragments) in 60 minutes but only 13% is mineralised to CO_2 and H_2O. Further, a
321 comparison with fig. 4(b) shows that both these processes are much slower that colour
322 removal, suggesting that destruction of the chromophore is rapid and complete, after which

323 the oxidation of the remaining moieties takes place more slowly, with some mineralisation.

324 Figure 5(b) shows the current efficiency and specific power consumption as a function of
325 time for the experiments in fig. 4(a). As can be seen, the current efficiency is ca 100% up to 5
326 min, and the power consumption correspondingly low at 8 kWh kg_{COD}^{-1}. However, at longer
327 times, there is a marked and sudden drop in the current efficiency, and a concomitant rise in
328 specific power consumption. Comparing with fig. 4(b) suggests this behaviour may be
329 interpreted in terms of the initial attack on easily oxidised chromophores; once these have
330 been removed (after 8 min), the remaining organic species are more recalcitrant.

331 In the beginning of the experiment when the dye concentration was high enough, the current
332 efficiency was 100% meaning that all the current was used to degrade the dye molecule, then
333 side reaction started to take place; including the generation of O_3 and O_2. 100% current
334 efficiency indicates that the applied current density was less than the limiting current density
335 and the degradation process is under current control (kinetically controlled) [5, 7], i_{lim} =
336 4.F.K_m.COD, where F is Faraday's constant, K_m is the mass transfer coefficient [5, 7] (in our
337 cell, $K_m = 1.3 \times 10^{-4}$ m s^{-1}). It may be clear that the limiting current density changes with the
338 COD value, so it is not fixed value. Applied current density higher than the limiting one
339 resulted in current efficiency less than 100%, and the degradation process is under the mass
340 transfer control[5, 7]. When the dye concentration is high enough, at the beginning of the test,
341 100% of the current will be used to generate oxidants that will be used for dye
342 decolourisation/degradation, sometime after that (about 5 min), the dye concentration become
343 less and mass transfer of the dye towards the electrode become crucial and the current is
344 enough now for side reactions (O_3, O_2,..) and the current efficiency is decreasing
345 exponentially. On the other hand, the specific power consumption increased as the dye
346 concentration decreased, due to degradation, reflecting that the fact the power is being

consumed for side reactions (ozone). Due to the fact that NATO anodes has only been used a few times for organic degradation, see Wang et al (4-Chlorophenol) [47] and Chen et al. (Phenol) [48], there is no real power cost estimation. In addition, those researchers used different anode sizes and cell configuration that make the comparison to our results even more difficult.

To confirm that side reactions were happening during the experiment shown in fig. 4(a), ozone was monitored at the outlet of the gas separator, and the results are shown in fig. 5(c) along with the variation in current during the experiment. As can be seen from fig. 5(c), ozone is generated after 3 min electrolysis, with increasing ozone current efficiency up to 8% at 16 minutes; whilst the current density falls steadily. Figures 5(b) and (c) suggests that, as the RB50 is consumed, OH radicals become available to form ozone [9, 24, 27, 30, 31].

From fig. 5(c), it may be seen that the current decreased with time from ca. 50 mA cm^{-2} to ca. 25 mA cm^{-2} during 16 minutes of the experiment; in order to ascertain the reason for this, the experiments discussed in the next section were carried out.

3.2.1 Reactivating the MEA

The current in fig. 4(c) not only decreased with time, but also it was much less than that observed during the ozone generation experiments at 2.7 V depicted in fig. 3(a). This may be due to: (i) poisoning of the anode, (ii) the membrane (Nafion) of the MEA becoming resistive and/or (iii) delamination of the MEA.

To investigate whether the anode had been poisoned and could be re-activated, ozone was generated using the MEA employed in the dye decolourisation experiments discussed above at 2.7 V under the same conditions using: (1) 1 M $HClO_4$ as anolyte with Millipore water as catholyte (see curves (ii) of figs. 5(a) and (b)), (2) 1 M $HClO_4$ as anolyte and catholyte (see

curves (iii) of figs. 5(a) and (b)), and (3) Millipore water again as anolyte and catholyte (see curves (iv) of figs. 5(a) and (b)). Curves (i) of figs. 5(a) and (b) represent the use of Millipore water as the anolyte and catholyte from fig 3(a). The currents and ozone current efficiencies observed as a function of time from these experiments are shown in figs. 6(a) and (b), respectively.

As may be seen from figs. 6(a) and (b), both the current and ozone current efficiency observed using Millipore water as anolyte and catholyte are significantly lower than the values observed prior to the dye decolourisation experiments, i.e. ca. 1.3 A compared to 3 A and ca. 4 % compared to ca. 30 % gaseous ozone current efficiency (see fig 3(b)). However, using 1 M $HClO_4$ as anolyte, with Millipore water or 1 M $HClO_4$ as catholyte, resulted in a current of 3 A and ozone current efficiency up to 33%. Replacing the anolyte and catholyte with Millipore water resulted in the current falling to ca. 1.5 A and ozone current efficiency to ca. 8%. Whilst plots (i) and (iv) do suggest some poisoning of the NATO anode which is ameliorated by electrolysis in acidic anolyte, it is clear that a major factor is the delamination of the MEA and consequent loss of ionic contact between anode and Nafion. The delamination of the MEA may have been enhanced by the fact that the anolyte was recycled at 240 cm^{-3} min^{-1} whilst the catholyte was static (see fig. 2); given the pump operated on the peristaltic principle, this could cause flexing of the Nafion. At the end of all the experiments in this paper, the MEA was removed from the polycarbonate cell, and areas of delamination could clearly be observed.

3.2.2 Intermediate formation

To confirm the formation of acids during the electrolysis of the dye solutions, IC was used to investigate the dye oxidation byproducts. Figure 7 shows the peak area of different byproducts obtained from the IC output as a function of electrolysis time. It may be seen

from the figure that organic and inorganic species were formed. The former were acetic acid and maleic acid; their concentration increased with electrolysis time, and the concentration of maleic acid increased up to a max after 30 min. The inorganic species were NO_2^-, NO_3^-, Br^- and SO_4^{2-}. The concentration of Br^- was constant concentration over the first 15 min of electrolysis, after which it decreased, suggesting the formation of OBr^- and/or Br_2. A detailed study of the intermediates and the dye oxidation mechanism is to follow in a subsequent paper.

4 Conclusions

Ozone current efficiencies as high as 33% and power consumption as low as 25 kWh kg^{-1} O_3 have been reported for the first time for the generation of ozone from Millipore water using an MEA – based cell with a NATO anode and Pt/Ti cathode separated by Nafion at room temperature in flow mode.

The same MEA was found to be efficient with respect to the decolourisation of RB50 solution, a dye that has not been studied before in the literature. 1000 mg dm^{-3} RB50 solution was completely decolourised within 8 minutes at 2.7 V, with a current efficiency of 100% and specific power consumption of 8 kWh kg_{COD}^{-1} in the first 5 minutes of electrolysis. The removal of COD and TOC required longer times. The formation of organic and inorganic by products was observed.

Acknowledgment

KZ would like to thank Damascus University / Syria for a scholarship and Newcastle University for funding.

Reference

[1] E. Petrucci, D. Montanaro, Chemical Engineering Journal. 174 (2011) 612.
[2] Y.M. Vera, R.J. de Carvalho, M.L. Torem, B.A. Calfa, Chemical Engineering Journal. 155 (2009) 691.
[3] J.B. Parsa, M. Abbasi, Acta Chim. Slov. 54 (2007) 792.
[4] C.A. Martinez-Huitle, E. Brillas, Applied Catalysis B-Environmental. 87 (2009) 105.
[5] C.A. Martínez-Huitle, S. Ferro, Chem. Soc. Rev. 35 (2006) 1324.
[6] G. Chen, Separation and Purification Technology. 38 (2004) 11.
[7] M. Panizza, G. Cerisola, Chem. Rev. 109 (2009) 6541.
[8] C. Comninellis, Electrochimica Acta. 39 (1994) 1857.
[9] P. Kariyajjanavar, N. Jogttappa, Y.A. Nayaka, Journal of Hazardous Materials. 190 (2011) 952.
[10] H. Zhou, D.W. Smith, Journal Environmental Engineering Science. 1 (2002) 247.
[11] P.A. Christensen, W.F. Lin, H. Christensen, A. Imkum, J.M. Jin, G. Li, C.M. Dyson, Ozone-Science & Engineering. 31 (2009) 287.
[12] Y.H. Wang, S.A. Cheng, K.Y. Chan, X.Y. Li, Journal of the Electrochemical Society. 152 (2005) D197.
[13] P.A. Christensen, K. Zakaria, T.P. Curtis, Ozone-Science & Engineering. 34 (2012) 49.
[14] P.A. Christensen, K. Zakaria, T. Yonar, H. Christensen, J. Electrochem. Soc. 160 (2013) H405.
[15] H. Shekarchizade, M.K. Amini, International Journal of Electrochemistry. 2011 (2011) 1.
[16] P.A. Christensen, T. Yoner, K. Zakaria, Ozone: Science & Engineering. 35 (2013) 149.
[17] P.A. Christensen, A. Imkum, Ozone-Science & Engineering. 33 (2011) 389.
[18] Y. Cui, Y. Wang, B. Wang, H. Zhou, K.Y. Chan, Z.Y. Li, J. Electrochem. Soc. . 156 (2009) E75.
[19] Y.H. Wang, S. Cheng, K.Y. Chan, Green Chemistry. 8 (2006) 568.
[20] L.M. Da Silva, D.V. Franco, L.G. Sousa, I.C. Goncalves, Journal of Applied Electrochemistry. 40 (2010) 855.
[21] A. AL-Kdasi, A. IDRIS, K. SAED, C.T. GUAN, Global Nest: the Int. J. 6 (2004) 222.
[22] T. Poznyak, P. Colindres, I. Chairez, J. Mex. Chem. Soc. 51 (2007) 81.
[23] M. Rivera, M. Pazos, M.A. Sanromán, Desalination. 274 (2011) 39.
[24] Y. Yavuz, A.S. Koparal, U.B. Ogutveren, J Chem Technol Biotechnol. 86 (2011) 261.
[25] E. Forgacs, T. Cserhati, G. Oros, Environment International. 30 (2004) 953.
[26] J.H.B. Rocha, A.M.S. Solano, N.S. Fernandes, D.R. Da Silva, J.M.P. Hernandez, C.A. Martınez-Huitle, Electrocatal. 3 (2012) 1.
[27] D. Montanaro, E. Petrucci, Chemical Engineering Journal. 153 (2009) 138.
[28] T. Robinson, G. McMullan, R. Marchant, P. Nigam, Bioresource Technology. 77 (2001) 247.
[29] E. Brillas, I. Sires, M. Oturan, Chem. Rev. 109 (2009) 6570.
[30] Y. Yavuz, R. Shahbazi, Separation and Purification Technology. 85 (2012) 130.
[31] E. Tsantaki, T. Velegraki, A. Katsaounis, D. Mantzavinos, Journal of Hazardous Materials. 207 - 208 (2012) 91.
[32] F. Montilla, E. Morallon, A. De Battisti, J.L. Vazquez, Journal of Physical Chemistry B. 108 (2004) 5036.
[33] A. Nemes, I. Fabian, G. Gordon, Ozone-Science & Engineering. 22 (2000) 287.
[34] A.D. Eaton, L.S. Clesceri, A.E. Greenburg, Standard Methods for the Examination of Water and Wastewater, 21st, American Public Health Association (APHA), Washinton D.C, 1998, 5220 C.

[35] E. Kusmierek, E. Chrzescijanska, M. Szadkowska-Nicze, J.K. Czaplinska, J Appl Electrochem. 41 (2011) 51.
[36] C.A. Martínez-Huitle, E.V.D. Santos, D.M.D. Araújo, M. Panizza, Journal of Electroanalytical Chemistry. 674 (2012) 103.
[37] M.I. Awad, M.M. Saleh, Journal of Solid State Electrochemistry. 14 (2010) 1877.
[38] A. Kraft, M. Stadelmann, M. Wunsche, M. Blaschke, Electrochemistry Communications. 8 (2006) 883.
[39] K. Kitsuka, K. Kaneda, M. Ikematsu, M. Iseki, K. Mushiake, T. Ohsaka, Electrochimica Acta. 55 (2009) 31.
[40] K. Arihara, C. Terashima, A. Fujishima, Electrochemical and Solid-State Letters. 9 (2006) D17.
[41] D. Gardoni, A. Vailati, R. Canziani, Ozone: Science & Engineering. 34 (2012) 233.
[42] K. Arihara, C. Terashima, A. Fujishima, Journal of the Electrochemical Society. 154 (2007) E71.
[43] K. Onda, T. Ohba, H. Kusunoki, S. Takezawa, D. Sunakawa, T. Araki, Journal of the Electrochemical Society. 152 (2005) D117.
[44] S. Stucki, H. Baumann, H.J. Christen, R. Kotz, Journal of Applied Electrochemistry. 17 (1987) 773.
[45] M. Faouzi, P. Canizares, A. Gadri, J. Lobato, B. Nasr, R. Paza, M.A. Rodrigo, C. Saez, Electrochimica Acta. 52 (2006) 325.
[46] J. Grebel, J.J. Pignatello, A. Mitch, Environ. Sci. Technol. 44 (2010) 6822.
[47] Y.H. Wang, K.Y. Chan, X.Y. Li, S.K. So, Chemosphere 65 (2006) 1087.
[48] Q.-Y. Chen, D.-D. Shi, Y.-J. Zhang, Y.-H. Wang, Water Science and Technology. 62 (2010) 2090.

Figure Captions

1. (a) The membrane electrode assembly and the polycarbonate (PC) electrochemical cell: (1) PC cell body, (2) NATO mesh anode spot-welded onto a Ti frame, (3) the Nafion 117 membrane, (4) the Pt/Ti mesh cathode spot-welded onto a Ti frame. (b) The cathode and anode meshes on the Ti frames.

2. Schematic of the decolourisation systems used for the decolourisation experiments using the MEA – based electrochemical cell.

3. (a) Plots of O_3 concentration as a function of cell voltage in (i) solution phase, (ii) gas phase and (iii) total (solution + gas) during an experiment in which Millipore water (as anolyte and catholyte) was electrolysed. The anolyte flow rate was 200 cm^3 min^{-1} in single pass, or flow, mode. The N_2 flow rate was 120 cm^3 min^{-1}. The catholyte was static. (b) Plots of: (i) current density, (ii) solution ozone current efficiency, (iii) gas phase ozone current efficiency and (iv) total ozone current efficiency vs. cell voltage during the experiments in fig. 3(a). (c) Plots of: (i) power consumption and (ii) ozone production rate vs. cell voltage observed during the experiments in fig. 3(a).

4. (a) UV – Vis spectra collected during the decolourisation of 200 cm^3 of 1000 mg dm^{-3} of RB50 in the MEA – based cell, the spectra were collected: (i) at the start of the electrolysis (t = 0), (ii) after 2 min and then every 2 min up to (ix) 16 min. (b) Plots of the removal efficiency vs. time of: (i) colour (λ_{max} = 625 nm), (ii) colour (λ_{max} = 586 nm) and (iii) benzene ring (λ_{max} = 254 nm). The cell voltage was 2.7 V, the N_2 flowrate 120 cm^3 min^{-1}, the anolyte flowrate was 200 cm^3 min^{-1}, at room temperature.

5. (a) Plots of: (i) COD removal and (ii) TOC removal vs. electrolysis time. (b) Plots of: (i) the current efficiency and (ii) the specific power consumption vs. electrolysis time.

(c) Plots of: (i) current density and (ii) ozone current efficiency as function of time observed during the experiments depicted in fig. 4(a).

6. (a) Plots of current as a function of time during the experiments conducted after those depicted in figs. 4(a). In each case, the anolyte flow rate was 200 cm^3 min^{-1} and the catholyte was static. (i) Millipore water as catholyte and anolyte represent data from fig 3(b) , (ii) 1 M $HClO_4$ as anolyte and Millipore water as catholyte, (iii) 1 M $HClO_4$ as catholyte and anolyte and (iv) Millipore water as anolyte and catholyte. The cell voltage was 2.7 V, at room temperature. (b) Plots of the ozone current efficiency vs. time for the experiments described in fig. 6(a). (i) - (iv) are as above in fig. 6(a).

7. Plots of the areas under the chromatographic peaks (determined using IC) as a function of electrolysis time for the byproducts observed during the experiment in fig 5(a). See text for details.

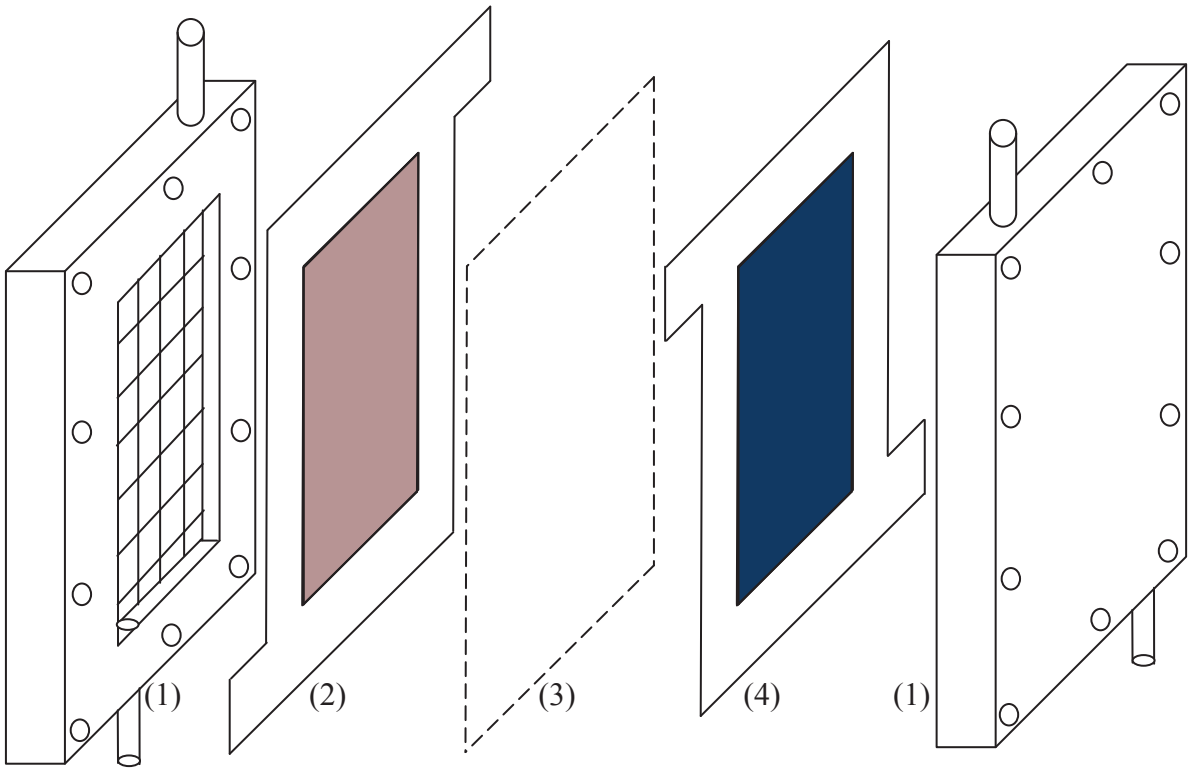

(a)

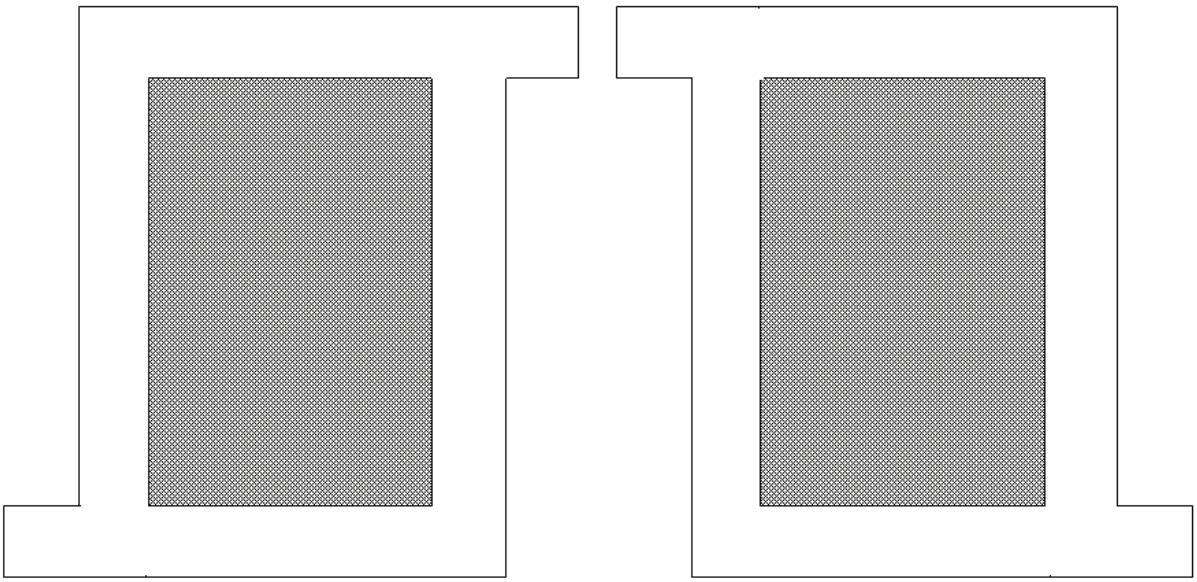

(b)

Figure 1.

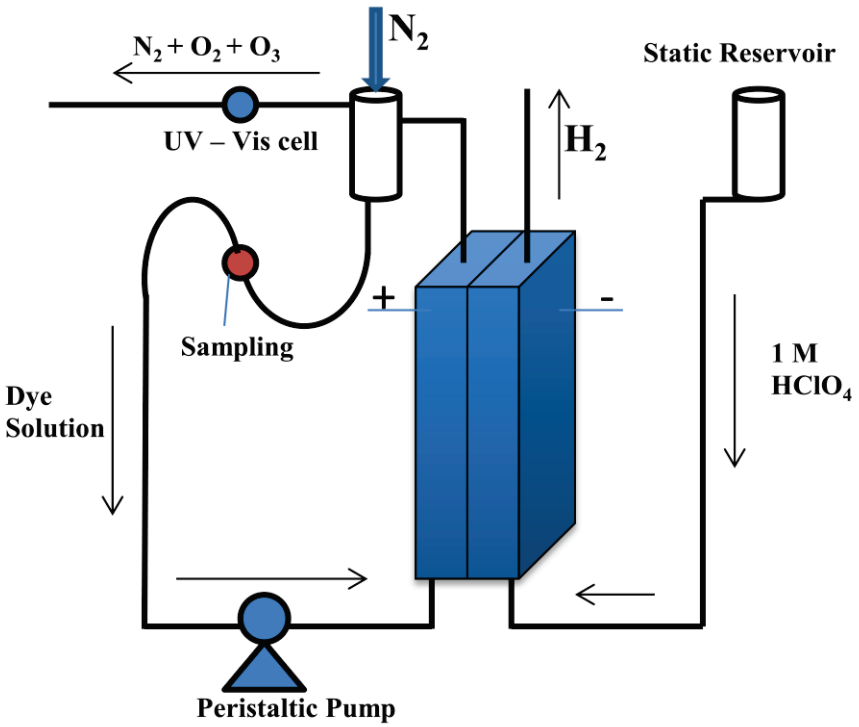

532
533
534
535
536 Figure 2.

537

538

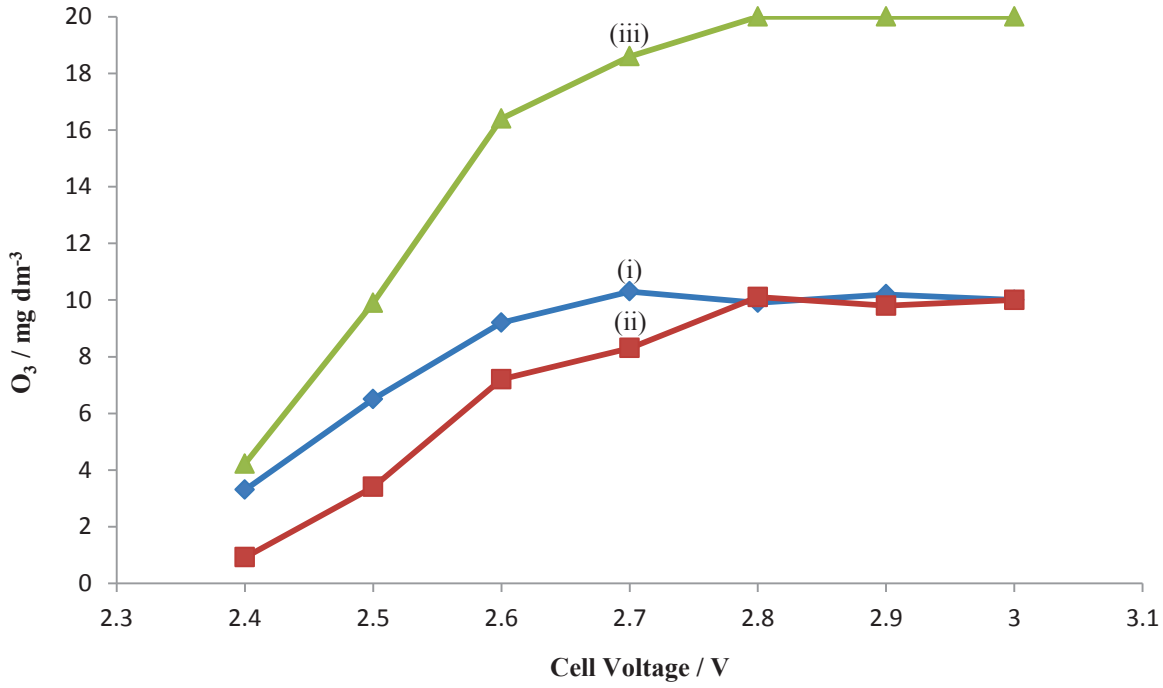

539

(a)

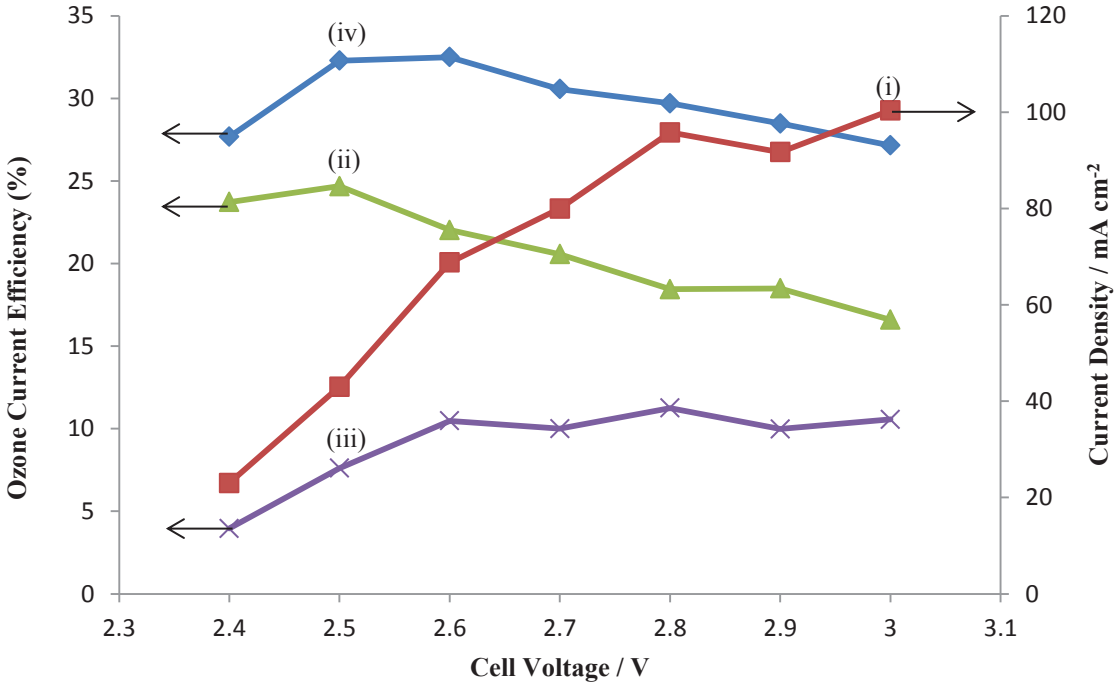
Ozone Current Efficiency (%)
Current Density / mA cm-2
Cell Voltage / V
(i)
(ii)
(iii)
(iv)

(b)

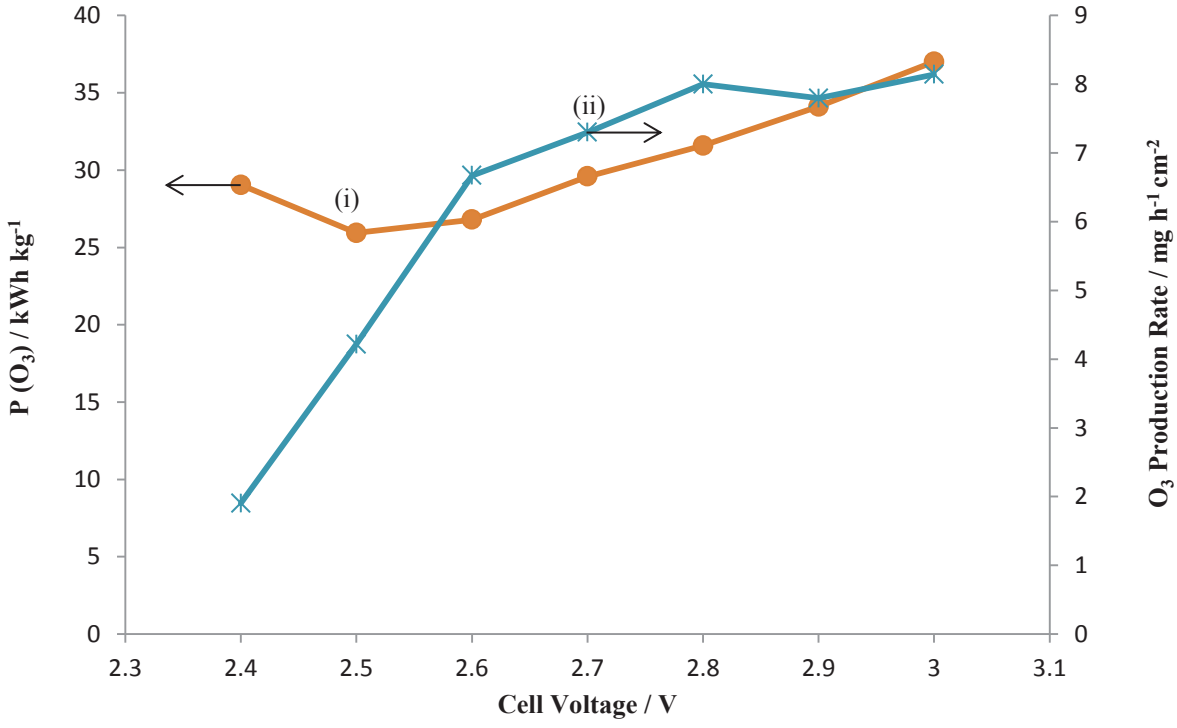
P (O3) / kWh kg-1
O3 Production Rate / mg h-1 cm-2
Cell Voltage / V
(i)
(ii)

(c)

Figure 3.

549

550

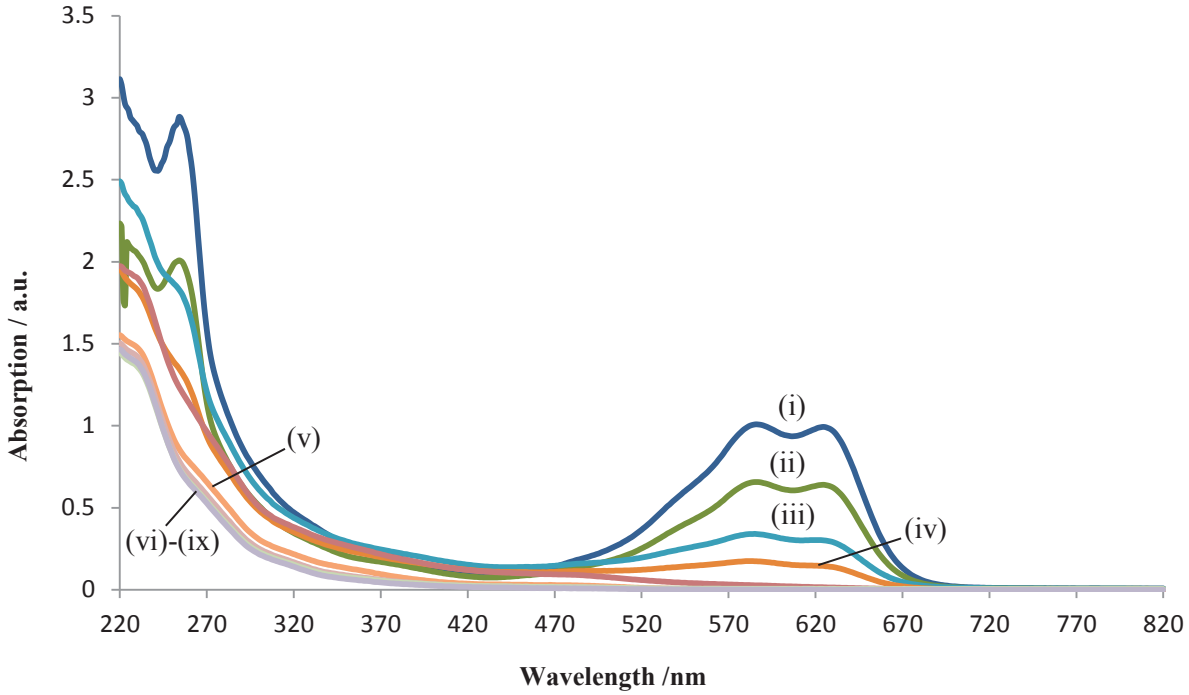

551

552 (a)

553

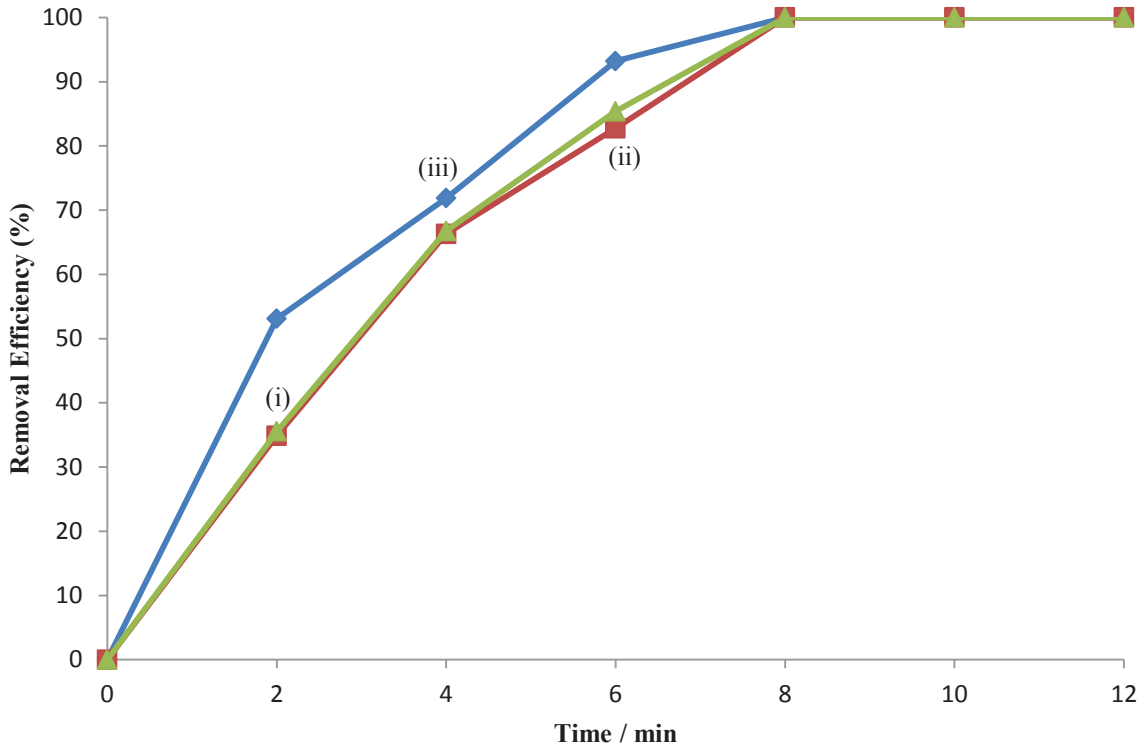

554
555 (b)

556 Figure 4.

557

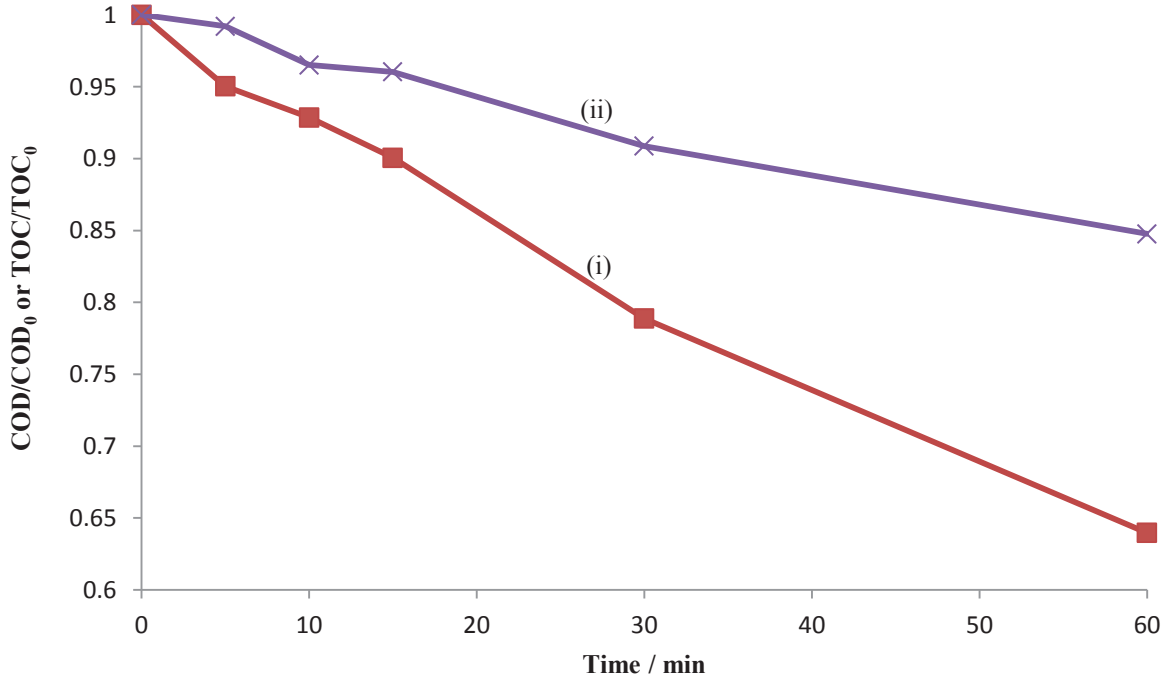

558

559 (a)

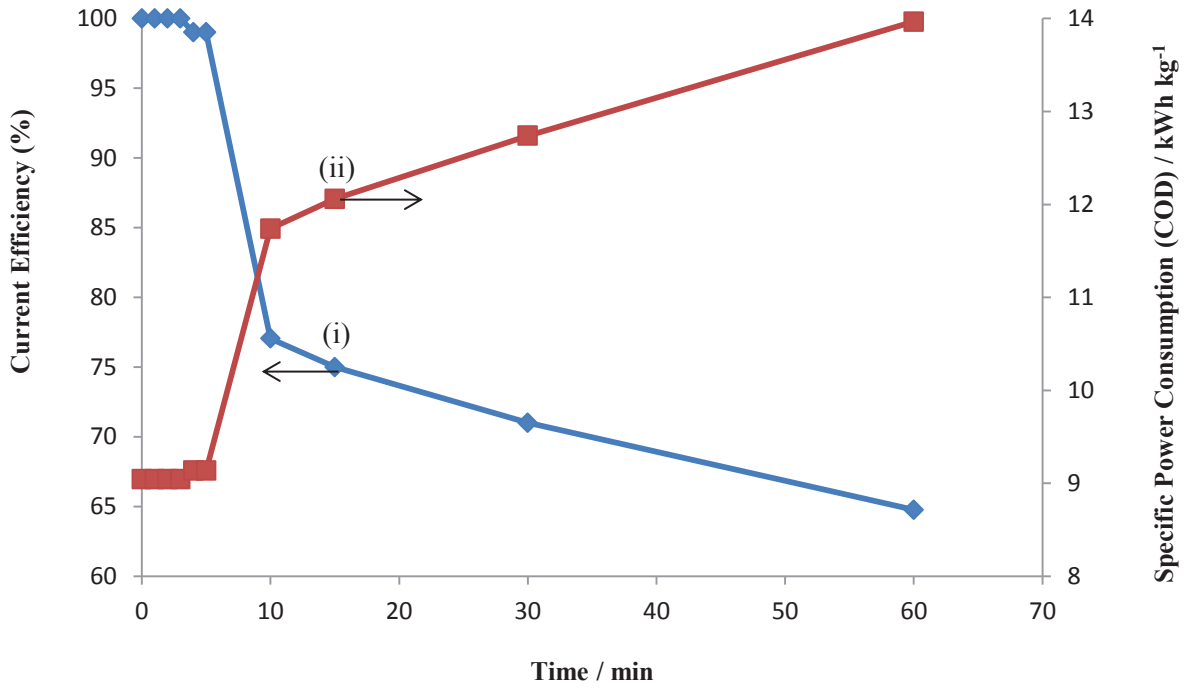

560

561 (b)

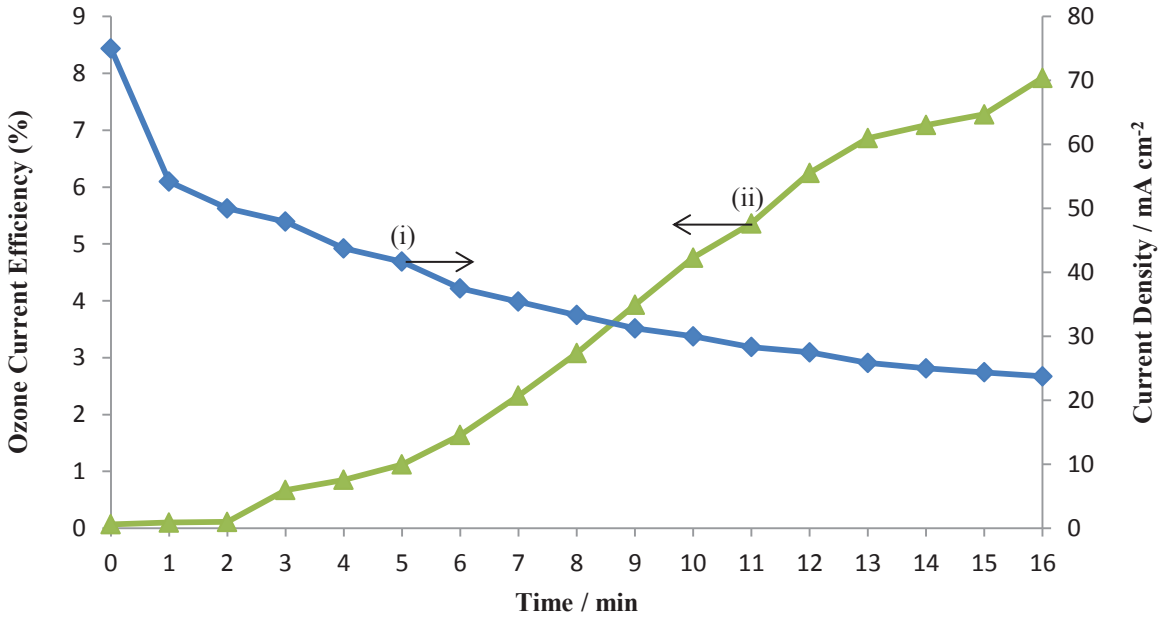

562
563 (c)

564 Figure 5.

565

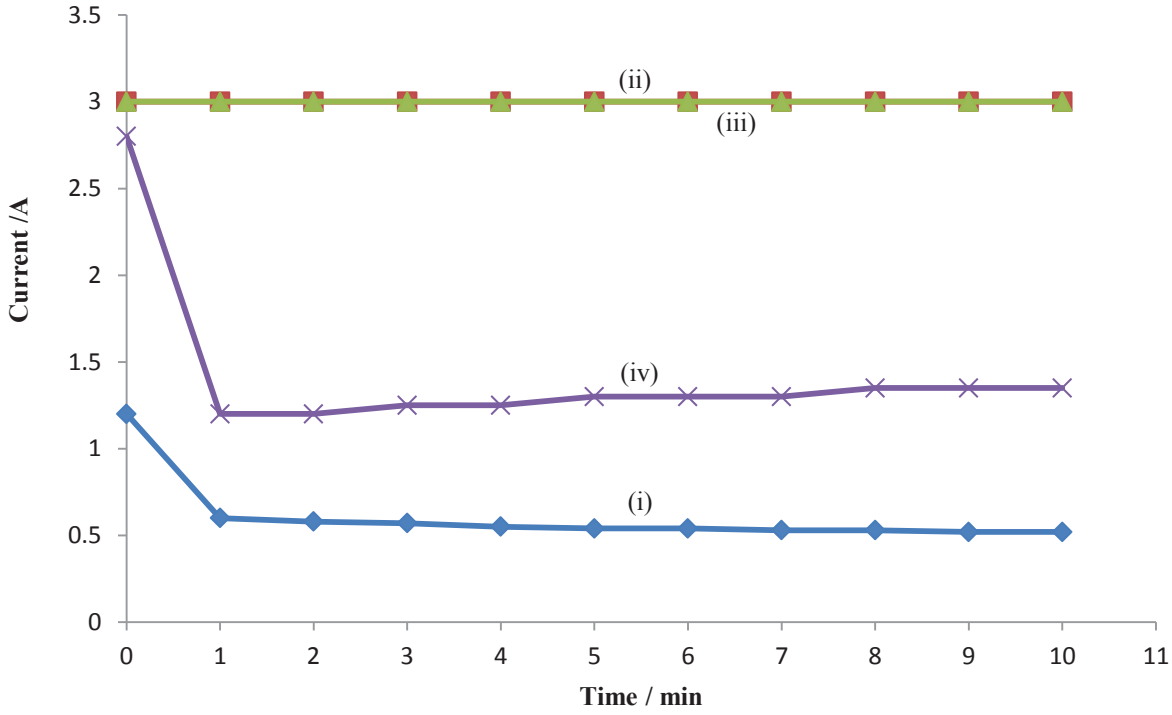
Current /A
Time / min
(i)
(ii)
(iii)
(iv)

(a)

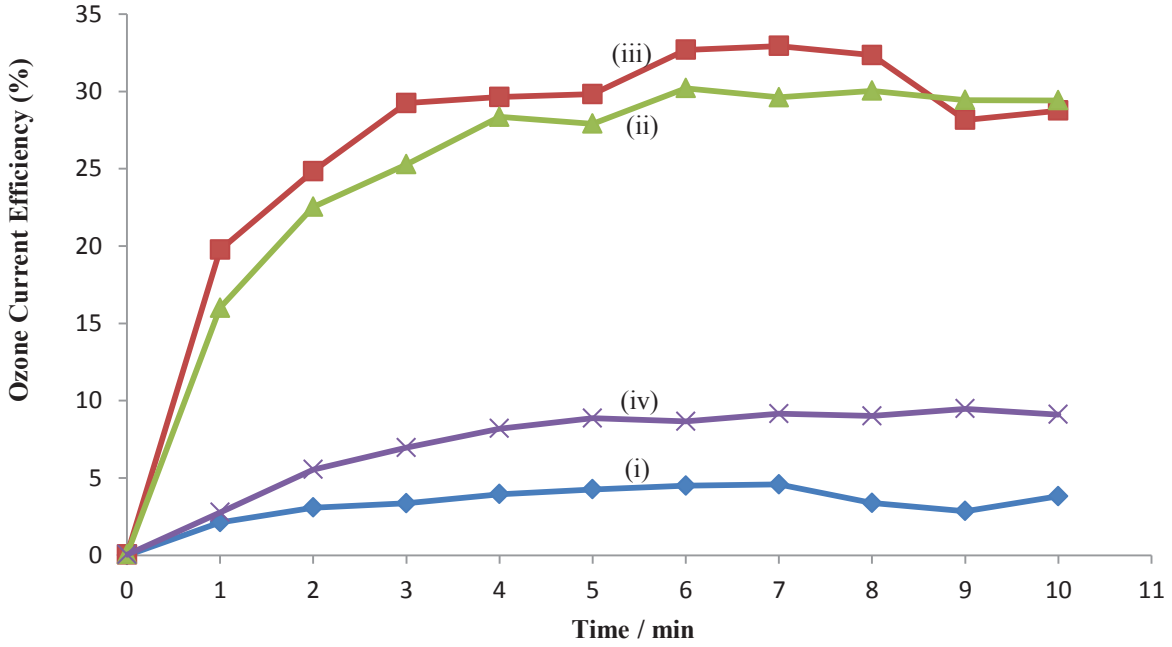
Ozone Current Efficiency (%)
Time / min
(i)
(ii)
(iii)
(iv)

(b)

Figure 6.

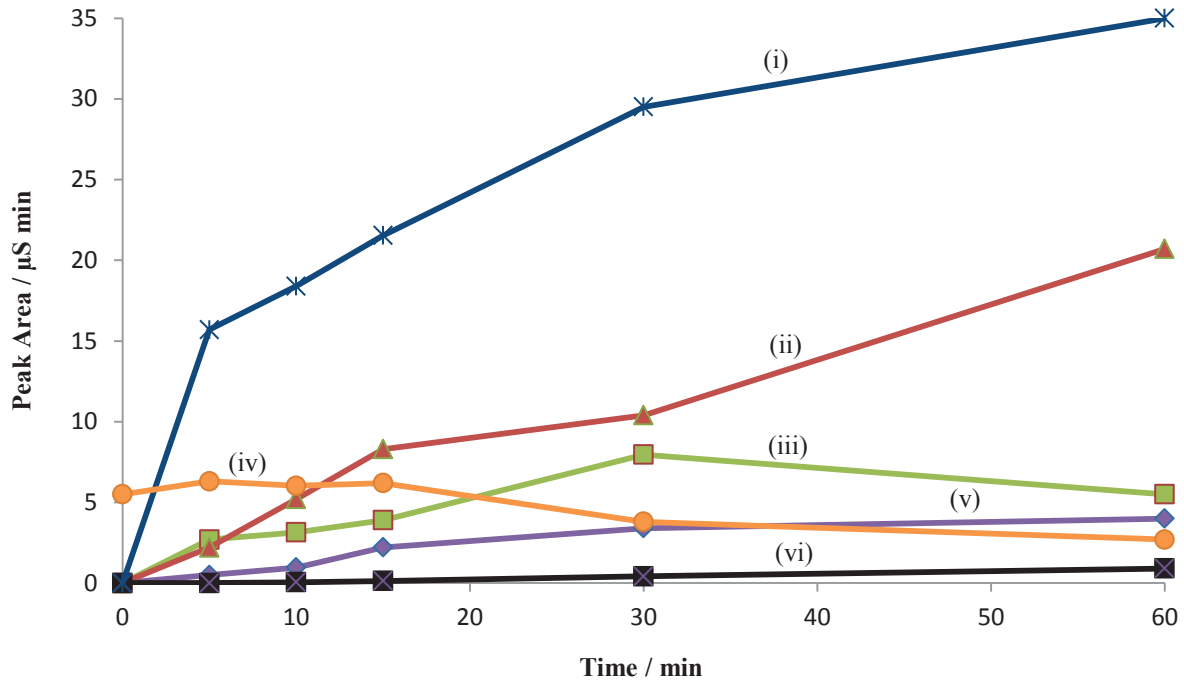

572

573 Figure 7.

574